Network dynamics and suppression of spray combustion instability in a backward-facing step combustor

Kenta Kato,[1] Hiroshi Gotoda,[1,*] Yusuke Nabae,[1] Maho Kawai,[2] and Ryoichi Kurose[2]

[1] *Department of Mechanical Engineering, Tokyo University of Science, 6-3-1 Niijuku, Katsushika-ku, Tokyo, 125-8585, Japan*

[2] *Department of Mechanical Engineering and Science, Kyoto University, Kyoto daigaku-Katsura, Nishikyo-ku, Kyoto, 615-8540, Japan*

(Received 19 December 2024; revised 12 April 2025; accepted 14 May 2025; published 1 July 2025)

We numerically study the network dynamics and suppression of spray combustion instability in a backward-facing step combustor from the perspective of a complex network. We observe the appearance, disappearance, and reappearance of a scale-free topology in a turbulence network. A scale-free topology appears when a large-scale organized vortex is formed, whereas it disappears upon the collapse of the organized vortex. A spatially irregular retention of primary hubs occurs in the turbulence network, which is closely associated with the collapse motion of a large-scale organized vortex. Spray combustion instability is significantly suppressed by placing an obstacle at the location where connector communities are mostly formed in the turbulence network.

DOI: 10.1103/zhkg-c3kh

I. INTRODUCTION

A self-excited thermoacoustic instability in combustors, referred to as combustion instability, occurs as a consequence of the high amplification of acoustic resonance modes due to the strong interactions among acoustic pressure, heat release rate, and flow velocity fields [1]. The unwanted high-amplitude acoustic pressure fluctuations during combustion instability impart vibrations to the combustor wall, leading to the fatal structural damage of combustors such as land-based and aero-derivative gas turbines. In these combustors consisting primarily of shear flows, the roll-up of the shear layer and the subsequent breakdown of vortices have considerable effects on the feedback coupling of fluctuations in acoustic pressure and heat release rate during combustion instability. The shear layer flow induced by a backward-facing step is one of the most fundamental flow fields for investigating the nonlinear dynamics of combustion instability. Many experimental and numerical studies [2–7] using backward-facing step combustors have clarified that an organized vortex driven by shear layer growth significantly affects combustion instability. Poinsot *et al.* [4] clarified the relationships among vortex shedding, acoustic, and heat release cycles. Schadow and Gutmark [6] reported that the mixing between unburned reactants and combustion products can produce a sudden heat release, leading to the reinforcement of the coupling in phase with the acoustic field during the formation of the organized vortex. George *et al.* [8] showed that the acoustic field progressively synchronizes with the organized vortex, leading to the formation of combustion instability. These studies collectively emphasize the importance of understanding how organized vortex dynamics affects flame behavior and thermoacoustic interactions in turbulent reacting flows.

The advent of network science [9,10] evolving from discrete mathematics has led to accelerated progress in the development of sophisticated complex networks: visibility graph [11], cycle network [12], recurrence network [13], transition network [14], and turbulence network [15]. Recent review papers [16,17] have shown the applicability of complex-network analysis as a powerful framework for capturing the behavior of flow structures in turbulent systems, providing new possibilities for interpreting the complex behavior of turbulent reacting flows. Substantial advances in complex-network analysis have importantly created a new interdisciplinary fusion between combustion dynamics and network science [18], providing a profound understanding of the dynamic behavior and physical mechanism of the incidence and sustainment of combustion instabilities [19–28]. Tandon and Sujith [29] have recently clarified the coupling between thermoacoustic power sources and coherent vortex structures using a multilayer network. They emphasize that the characterization of how such structures form and evolve is essential to understanding the onset and suppression of combustion instability.

Spray combustion is a well-recognized chemically reacting two-phase turbulent flow with complex elementary processes involving fuel atomization, droplet dispersion,

*Contact author: gotoda@rs.tus.ac.jp

and droplet evaporation. A research group from Kyoto University [30–32] has recently conducted numerical studies on spray combustion instability in a backward-facing step combustor by large-eddy simulation (LES). The studies focused mainly on clarifying the effects of temporal evolutions of fuel droplet diameter distribution and fuel flow rate on the intensity of acoustic pressure fluctuations and the local Rayleigh index. We have recently studied the dynamical state and driving region of spray combustion instability in a backward-facing step combustor [33] using a transition network and an acoustic-energy-flux-based spatial network [34]. Our main findings obtained by the complex-network analysis are as follows: (1) the global dynamical state of acoustic pressure fluctuations (heat release rate fluctuations) represents a limit cycle (low-dimensional chaotic oscillations); (2) the irregular formation of hubs in the spatial network contributes significantly to the emergence of chaotic oscillations; and (3) the formation and loss of thermoacoustic power sources are closely related to a large-scale organized vortex motion. These findings have provided us with a new perspective on understanding the dynamical state and driving region of spray combustion instability.

Our main interest and motivation in this study are to clarify the network dynamics and construct a useful method to suppress spray combustion instability, focusing on a large-scale organized vortex motion. As mentioned above, we have recently elucidated a strong association between the formation and loss of thermoacoustic power sources and a large-scale organized vortex [33]. Building on this, we explore an approach to modifying the flow field by disrupting the vortical structures to reduce the generation of thermoacoustic power sources. One of the promising networks is the turbulence network, which enables us to perceive the constitutive behavior of the vortical structure during combustion instability [22,25,28,35,36]. The potential utility of the turbulence network is the extraction of the topological structure hidden in the underlying combustion dynamics and of the driving region of combustion instability, which is difficult to identify by the vorticity field. Murayama *et al.* [22] have shown the existence of a scale-free topology and identified a primary hub in the turbulence network during combustion instability in a swirl-stabilized combustor. Kurosaka *et al.* [35] have also shown that the loss of the primary hub plays a critical role in suppressing combustion instability in the same combustor [22]. Krishnan *et al.* [25] reported the existence of a scale-free topology in the turbulence network during combustion instability in a bluff body–stabilized combustor, highlighting the prevention of primary hubs to suppress combustion instability. Zheng *et al.* [28] clarified a nontrivial relationship between a scale-free topology in the turbulence network and acoustic pressure fluctuations, exhibiting the continuous sustainment of a scale-free topology during combustion instability in a bluff body–stabilized swirling combustion system. On the basis of these studies [22, 25,28,35], in this study, we clarify a scale-free topology in the turbulence network during spray combustion instability.

A community is a group of nodes that exhibit stronger internal connections than external connections in a network. The *P-Z* plane consisting of the within-module degree and the participation coefficient [37] enables the identification of dominant module nodes within a classified community during combustion instability [34,36]. Sahay *et al.* [38] have recently shown that community structures in the turbulence network help characterize interactions among vortical structures. The intercommunity interactions correlate with acoustic pressure fluctuations in a turbulent combustor. On the basis of this point, our study examines how the formation and collapse of an organized vortex affect the structure of the turbulence network, focusing particularly on the role of connector communities in modulating spray combustion instability. We extract connector communities in the turbulence network by estimating the participation coefficient. We finally attempt to suppress spray combustion instability by placing an obstacle in the extracted region of the connector communities.

The rest of this paper is organized as follows: Numerical computation and analytical methods are explained in Sec. II. Results and discussion are provided in Sec. III. The findings are summarized in Sec. IV.

II. NUMERICAL COMPUTATION AND ANALYTICAL METHODS

We conduct the complex-network analysis of the spatiotemporal data [33] of spray combustion instability obtained by LES. The governing conservation equations consisting of the mass, momentum, energy, mass fraction of chemical species, state equation for the ideal gas, and boundary conditions are nearly the same as those in previous studies [30–32]. Our LES has been conducted with finer spatial resolutions than in the above-mentioned studies [30–32]. Figure 1 shows the external view of a backward-facing step combustor and the computational domain and conditions. Air is supplied from the combustor inlet. Fuel droplets of kerosene [30–32] are supplied vertically upward approximately 5 mm upstream from the edge of the step, where the height of the step is approximately 19.1 mm. Similarly to in our recent study [33], the equivalence ratio is set to 1.2. The cross-section velocity U and temperature T of the incoming air are set to 50 m/s and 760 K, respectively. The initial vertical velocity V_f and temperature T_f of the incoming fuel droplets are 2 m/s and 300 K, respectively, and the initial pressure inside the combustor is set to 0.1 MPa. The process for atomization of liquid fuel follows a model considering the dynamical changes in the initial droplet-size profiles

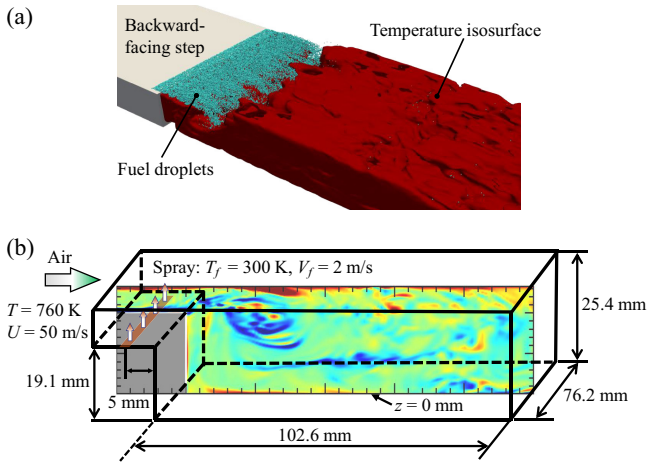

FIG. 1. (a) External view of a backward-facing step combustor during spray combustion instability and (b) computational domain and conditions.

[39]. A nonequilibrium Langmuir-Knudsen model [40–42] is adopted for the evaporation process. As shown in Fig. 1(a), the fuel droplets (green dots) are transported downstream by the incoming air. They burn accompanied by the engulfment of an organized vortex [see the instantaneous vorticity field in Fig. 1(b)]. Note that the dominant frequency of the spatially averaged acoustic pressure fluctuations $\langle p \rangle$ is approximately 700 Hz [33] during spray combustion instability, which almost corresponds to a quarter of the wavelength mode in a backward-facing step combustor [31].

A turbulence network as proposed by Taira *et al.* [15] is a vortex interaction–based undirected and weighted network. In this study, we estimate the node strength in the turbulence network constructed from the vorticity field in $z \approx 0$ and $-1 \leq x/H \leq 7$. Each computational grid is a node in the network, and the links between nodes are connected by the magnitude of the induced velocity. The induced velocity refers to the effect of one fluid element on another and is calculated with use of the Biot-Savart law. This law represents the flow velocity generated by a vortical element as a function of its circulation and distance between vortical elements. The induced velocity u_{ij} from node i to node j is calculated as

$$u_{ij} = \frac{|\omega(\mathbf{x}_i)\,\Delta x_i \Delta y_i|}{2\pi\,|\mathbf{x}_i - \mathbf{x}_j|}, \tag{1}$$

where $\mathbf{x}_i$ is the position vector of the ith node, $\omega(\mathbf{x}_i)$ is the vorticity, and Δx_i (Δy_i) is the grid size in the x (y) direction. The interaction between nodes is quantified by our taking the average of induced velocities between vortices. Thus, the weighted adjacency matrix $A_{t,ij}$ in the turbulence network is defined as

$$A_{t,ij} = \begin{cases} \frac{1}{2}\left(u_{ij} + u_{ji}\right) & \text{if } i \neq j, \\ 0 & \text{otherwise.} \end{cases} \tag{2}$$

We can finally estimate the node strength $s_{t,i}$ in the network as

$$s_{t,i} = \sum_{j=1}^{N} A_{t,ij}, \tag{3}$$

where N is the number of nodes and is 15 325 in this study. The node strength in the turbulence network quantifies the interactions between a fluid element and its surrounding flow. High node strength indicates regions where vortical interactions are particularly strong, signifying the presence of dominant organized structures. In contrast, low node strength indicates regions where interactions with the surrounding flow are relatively weak. Note that in our preliminary test, the key turbulent structures involving a large-scale organized vortex are sufficiently captured when the analytical domain is changed to $-1 \leq x/H \leq 5$. The essential features of the flow field are well represented at the chosen number of nodes.

We examine the presence of a scale-free topology in the turbulence network by analyzing the probability density function of node strength. A scale-free topology appears in the network if the node strength distribution follows a power-law relationship:

$$P(s_{t,i}) \sim s_{t,i}^{-\gamma}, \tag{4}$$

where γ is the scaling exponent. The power-law distribution shows that most nodes have low strength, while a small fraction of nodes (hubs) possess significantly higher strength, indicating the self-organization in the flow field. We estimate the coefficient of determination R^2, which quantifies how well the log-transformed data follow a linear trend:

$$R^2 = 1 - \frac{\sum_i \left(\log P(s_{t,i}) - \log \hat{P}(s_{t,i})\right)^2}{\sum_i \left(\log P(s_{t,i}) - \overline{\log P(s_{t,i})}\right)^2}, \tag{5}$$

where $\hat{P}(s_{t,i})$ is the value of $P(s_{t,i})$ predicted from the regression, and $\overline{\log P(s_{t,i})}$ is the average of the logarithmic $P(s_{t,i})$. A value of R^2 close to unity means a high degree of consistency with the power-law distribution, indicating the presence of a scale-free topology. Similarly to Ref. [22], we define a scale-free topology as being present when $R^2 > 0.90$.

Guimerà and Amaral [37] proposed the P-Z plane method for the identification of influential nodes through

intracommunity and intercommunity interactions in a network. Meena and Taira [43] identified the network connector and peripheral nodes by assessing the strengths of the community interactions among groups of vortical nodes in the turbulence network. In accordance with their studies [37,43], we identify a connector community in the turbulence network. A connector community represents a set of nodes that establish strong connections between different communities within the network. Similarly to what was done in recent studies [34,36], communities are extracted by the Louvain method [44,45]. The Louvain method is an optimization algorithm designed to maximize the modularity Q_m of the network. The modularity Q_m quantifies the strength of division into communities by comparing the observed connectivity within communities with a network model where connections are randomly distributed. However, the Louvain method focuses on intracommunity cohesion and does not explicitly consider interactions between different communities. We thus introduce the concept of connector communities, which are defined as subsets of Louvain-based communities that facilitate strong intercommunity interactions. After calculating the sum of the weights of the links adjacent to the nodes in the community m at the ith node, $s_{t,i,m}$, we estimate the participation coefficient P_i at the ith node. Note that $0 < P_i < 1$ and P_i reaches unity when the weights of the links connected to the ith node are homogeneously connected among all communities.

$$s_{t,i,m} = \sum_{j=1,\, c_j \in \hat{C}_m}^{N} A_{t,ij}\,, \tag{6}$$

where $\hat{C}_m$ is the set of the mth community.

$$P_i = 1 - \sum_{m=1}^{N_c} \left(\frac{s_{t,i,m}}{s_{t,i}} \right)^2, \tag{7}$$

where N_c is the total number of communities. In the connector communities, $\langle P_m \rangle$, denoting the average of P_i for each community m, takes the maximum value in all communities. In this study, we estimate the number of connector communities N_{CC}. It serves as an indicator to identify turbulent regions where interaction between vortical structures is particularly strong. These regions play a crucial role in the dynamics of combustion instability.

III. RESULTS AND DISCUSSION

Figure 2 shows the instantaneous spatial distribution of the node strength $s_{t,i}$ and the probability density function $P(s_{t,i})$ of the node strength in the turbulence network. We observe high $s_{t,i}$ values near the core of the rolled-up structure of a large-scale organized vortex ($0.5 \leq x/H \leq 1.2$, $0.5 \leq y/H \leq 0.9$) at $t = 135.67$ ms. An important point to note here is that the region with high $s_{t,i}$ nearly corresponds to that in the acoustic-energy-flux-based spatial network we have presented recently [33]. This suggests that a large-scale organized vortex with the engulfment of fuel droplets is indispensable for the significant production of thermoacoustic energy. As shown in Fig. 2(B) (a), $P(s_{t,i})$ exhibits a power-law decay. The coefficient of determinism R^2 at $t = 135.67$ ms is estimated to be approximately 0.96 and the spatial scaling exponent γ is -2.6. This indicates that a scale-free topology appears when a large-scale organized vortex is formed. In contrast, when $t = 136.17$ ms, corresponding to the collapse time of a large-scale organized vortex, $P(s_{t,i})$ appears to be scattered for $s_{t,i} > 8 \times 10^2$, and R^2 is approximately 0.74, indicating the disappearance of the scale-free topology. These results demonstrate that a scale-free topology of the turbulence network is closely associated with the organized vortex motion. In a scale-free network, a small fraction of nodes (hubs) dominate the overall connectivity of the network. In the turbulence network, these hubs are located predominantly in regions of intense flow interactions, such as the vortex core and shear layer. When a large-scale organized vortex forms, these regions establish strong connections with other parts of the network, acting as a critical effect that sustains the

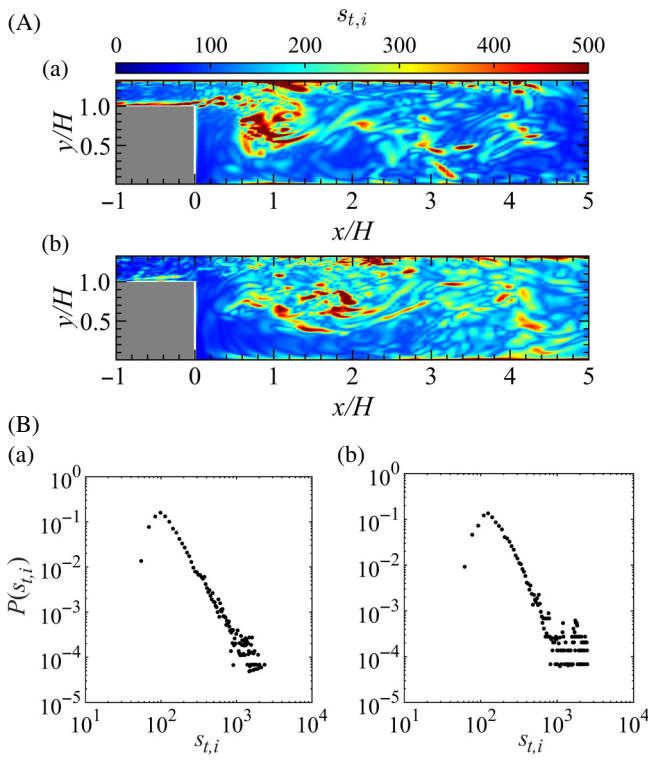

FIG. 2. (A) Instantaneous spatial distribution of node strength $s_{t,i}$ and (B) probability density function of $s_{t,i}$ in the turbulence network during spray combustion instability. (A) (a),(B) (a) $t =$ 135.67 ms and (A) (b),(B) (b) $t = 136.17$ ms.

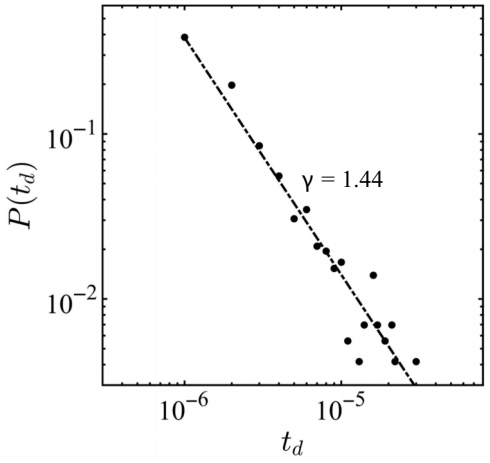

FIG. 3. Probability density function of the lifetime $P(t_d)$ of the scale-free topology in the turbulence network during spray combustion instability.

scale-free topology. The probability density function of the lifetime $P(t_d)$ is shown in Fig. 3, where t_d is the lifetime of the scale-free topology. We find a power-law decay with a scaling exponent of -1.44. This clearly shows that the substantivity of the scale-free topology can be characterized by the probability density function of the lifetime of the scale-free topology. Our discovery of the appearance, disappearance, and reappearance of a scale-free topology during spray combustion instability extends our understanding of network dynamics beyond that from a previous study [28], which focused on the continuous sustainment of the scale-free nature during gaseous combustion instability.

Figure 4 shows the spatiotemporal evolution of the average node strength $\langle s_{t,i}\rangle_y$ with respect to y, together with representative node strength fields. We observe that $\langle s_{t,i}\rangle_y$ exhibits temporally periodic fluctuations near the formation region of a large-scale organized vortex. The interval of the periodic $\langle s_{t,i}\rangle_y$ in response to the regular release of the organized vortex corresponds to the period of a quarter-wavelength mode of an acoustic wave in a backward-facing step combustor [31]. This behavior of $\langle s_{t,i}\rangle_y$ suggests that the turbulence network effectively captures the periodic emergence and collapse of a large-scale organized vortex. Although traditional analyses of vortex behavior often rely on flow velocity and vorticity fields, the result presented above demonstrates that the turbulence network serves as an effective complex network for extracting the temporal behavior of dominant vortical structures. This function will be particularly significant for various combustors where a large-scale organized vortex plays a crucial role in the formation and sustainment of combustion instability. The periodic behavior of node strength indicates that the topology of the turbulence network is dynamically coupled to the underlying flow behavior. This provides an encompassing understanding of network dynamics in more general vortex-driven combustion instabilities that are not limited to spray combustion instabilities. Our approach to extracting the spatiotemporal pattern of the node strength in a turbulence network has potential use in analyzing a wide range of problems in fluid mechanics where a large-scale organized vortex plays a crucial role in thermoacoustics. We also observe high $\langle s_{t,i}\rangle_y$ values from the vicinity of the backward-facing step edge to the formation region of the organized vortex, indicating the formation of primary hubs with a disproportionately large number of links. Such hubs dictate the behavior of the overall network. Although high-node-strength regions appear in roughly the same spatial extent, their persistence range does not remain constant owing to the collapse motion of a large-scale organized vortex.

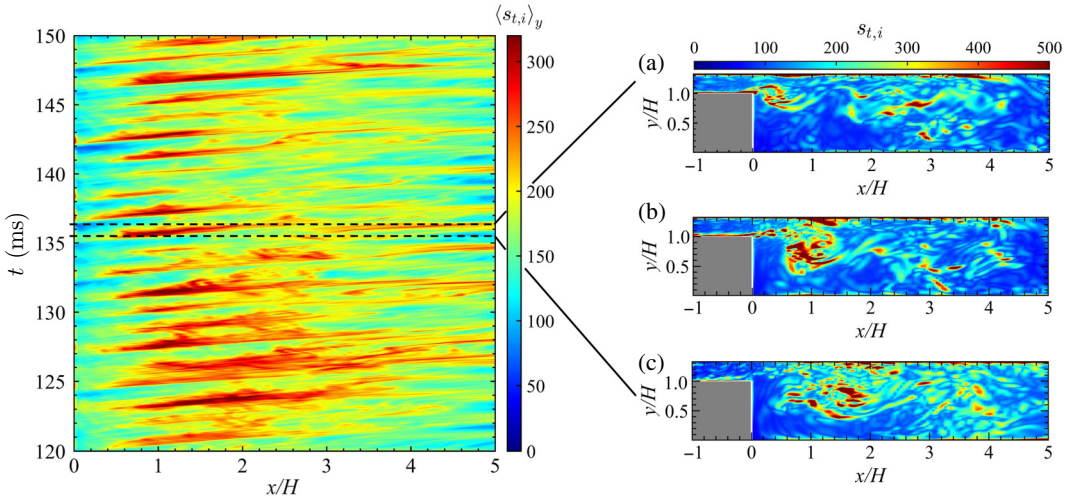

FIG. 4. Spatiotemporal evolution of the average node strength $\langle s_{t,i}\rangle_y$ with respect to y in the turbulence network, together with extracted representative node strength fields. (a) $t = 135.3$ ms, (b) $t = 135.7$ ms, and (c) $t = 136.1$ ms.

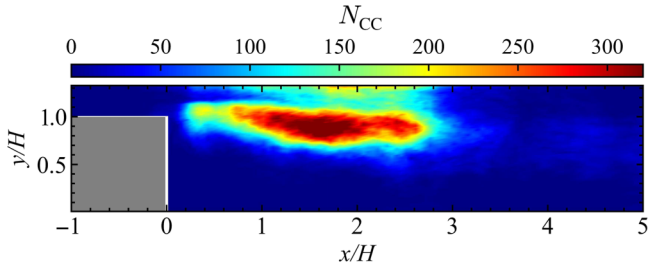

FIG. 5. Spatial distribution of the number of connector communities N_{CC} in the turbulence network during spray combustion instability.

Note that in this study, we regard such behavior of $\langle s_{t,i}\rangle_y$ downstream as a spatially irregular behavior. As mentioned in Sec. I, we have recently shown that the dynamical state of the global heat release rate field represents chaotic oscillations with deterministically nonperiodic intercycle dynamics [33]. We also have shown that the irregular formation of primary hubs in the acoustic-energy-flux-based spatial network serves a pivotal role in the emergence of chaotic oscillations in the heat release rate field. On the basis of that study [33] and the results shown in Fig. 2, we consider that the spatially irregular behavior of $\langle s_{t,i}\rangle_y$ associated closely with the loss of the scale-free topology also contributes significantly to chaotic oscillations in the heat release rate field during spray combustion instability.

Figure 5 shows the spatial distribution of the number of connector communities N_{CC}. Here, N_{CC} has the maximum value of $\langle P_k\rangle$. In the regions $0.8 \le x/H \le 2.8$ and $0.7 \le y/H \le 1.1$, N_{CC} takes high values, which indicates the formation of connector communities with a central role in the network. Krishnan *et al.* [25] have recently reported that the node strength in the turbulence network is useful for appropriately determining the location of steady secondary air jets to suppress combustion instability in a bluff body–stabilized combustor. We here attempt to suppress spray combustion instability by placing a rectangular obstacle with sizes of $1.6 \le x/H \le 1.8$ and $0.82 \le y/H \le 0.9$ in the formation region of the connector communities. Note that the setting location of the obstacle [see Fig. 6(a)] is rigorously determined to cover the region where N_{CC} is larger than 95% of the maximum N_{CC}. Figure 6(b) shows the temporal evolution of the spatially averaged acoustic pressure fluctuations $\langle P\rangle$ and the power spectral density (PSD) in cases without and with the obstacle. Both the amplitude of $\langle P\rangle$ and the dominant peak value of PSD in the case with the obstacle are smaller than those in the case without the obstacle. This indicates that spray combustion instability can be suppressed by placing an obstacle at the location where the connector communities are mostly formed. Figure 7 shows the temporal evolution of the spatially averaged node strength $\langle s_{a,i}\rangle$ in the acoustic-energy-flux-based spatial network in the cases

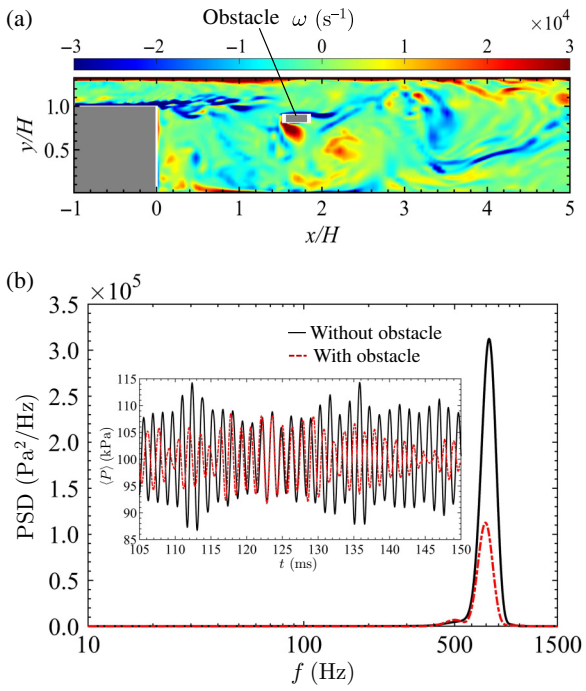

FIG. 6. (a) Instantaneous vorticity field ω inside a backward-facing step combustor with the obstacle at $t = 126.45$ ms and (b) temporal evolution of the spatially averaged acoustic pressure fluctuations $\langle P\rangle$ and the power spectral density in the cases without and with the obstacle. The sizes of the obstacle are $1.6 \le x/H \le 1.8$ and $0.82 \le y/H \le 0.9$.

without and with the obstacle, together with representative instantaneous fields of $s_{a,i}$ (see Ref. [33] for details of the acoustic-energy-flux-based spatial network). As shown in the instantaneous fields of $s_{a,i}$, the high $s_{a,i}$ values in the case without the obstacle are substantially diminished near the obstacle, preventing the formation of a thermoacoustic power source. The amplitude of $\langle s_{a,i}\rangle$ markedly decreases with the installation of the obstacle. The collapse of the connector communities leads to the suppression of spray combustion instability.

The recurrence rate in symbolic recurrence plots (SRPs) [13] is an important measure for evaluating the similarity between two time series. Gotoda and co-workers have evaluated the similarity of the acoustic pressure and heat release rate fluctuations during combustion instability in a swirl-stabilized combustor [26,46] and a model rocket engine combustor [47]. On this basis, we examine the degree of synchronized state between the spatially averaged acoustic pressure $\langle P\rangle_y$ and the heat release rate fluctuations $\langle Q\rangle_y$ by estimating the recurrence rate $R_{SR} = (1/(N_D - |\tau_l|)) \sum_{i=1}^{N_D-|\tau_l|} S_{R,ij}$. SRPs are constructed on the basis of the rank-order patterns of $\langle P\rangle_y$ and $\langle Q\rangle_y$. Here, $j = i + \tau_l$, N_D is the number of data points in the phase space, τ_l is the distance between the main diagonal and the parallel diagonals in the SRPs, and $S_{R,ij}$ represents an

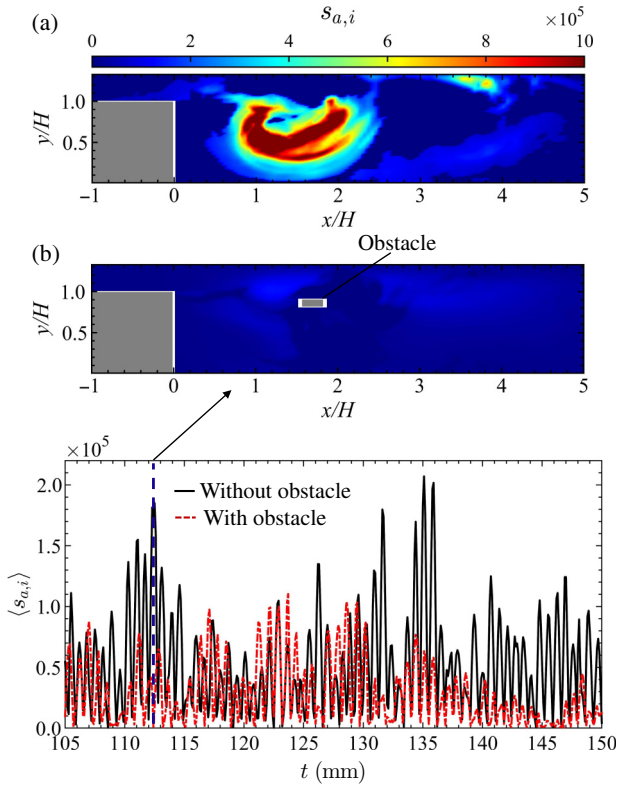

FIG. 7. Temporal evolution of the spatially averaged node strength $\langle s_{a,i} \rangle$ in the acoustic-energy-flux-based spatial network in the cases without and with the obstacle, together with representative instantaneous fields of $s_{a,i}$ at $t = 112.6$ ms. (a) Instantaneous field of $s_{a,i}$ in the case without the obstacle and (b) instantaneous field of $s_{a,i}$ in the case with the obstacle.

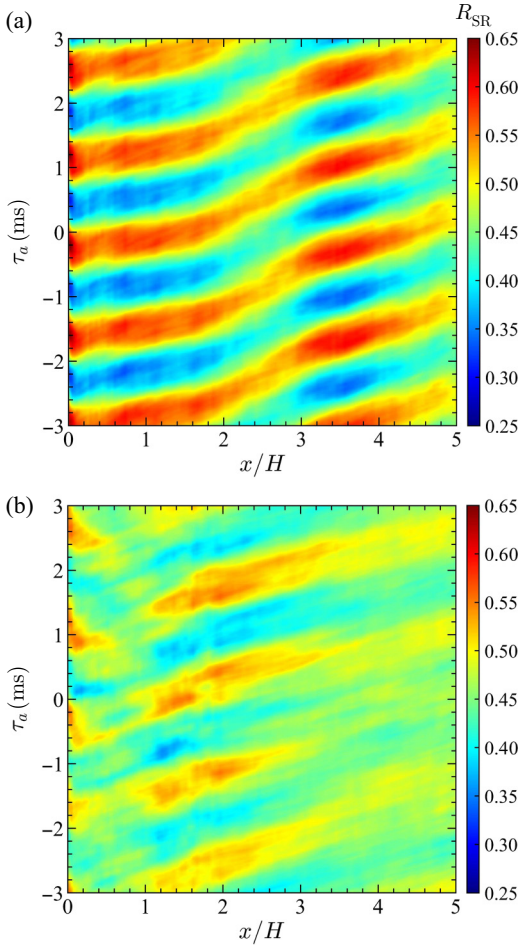

FIG. 8. Variation of the recurrence rate R_{SR} in symbolic recurrence plots as a function of x/H and the actual delay time τ_a. (a) In the case without the obstacle and (b) in the case with the obstacle.

element of the adjacency matrix, which is unity when the rank-order patterns of $\langle P \rangle_y$ and $\langle Q \rangle_y$ are identical, and is zero otherwise. A high R_{SR} value means a strongly phase-synchronized state between acoustic pressure and heat release rate fluctuations. The variation of R_{SR} in the cases without and with the obstacle is shown in Fig. 8 as a function of x/H and the actual delay time $\tau_a = \tau_l \Delta t$, where τ_l is the time distance between the main diagonal line and the parallel diagonal line in the recurrence plots and Δt is the time resolution of $\langle P \rangle_y$ and $\langle Q \rangle_y$. In the case without the obstacle, R_{SR} is periodically high in terms of τ_a, indicating the formation of a phase-synchronized state. The interval of neighboring maximum values of R_{SR} in terms of τ_a is approximately 1.38 ms, which corresponds to that of the temporally regular appearance of high $\langle s_{t,i} \rangle_y$ in the turbulence network (see Fig. 4). When the obstacle is placed at the location determined by the extraction of the connector communities, R_{SR} notably decreases with the changes in both x/H and τ_a. The periodicity of R_{SR} also decreases in terms of x/H. The installation of the obstacle weakens the phase-synchronized state. The results shown in Figs. 6–8 demonstrate that placing an obstacle in the region where connector communities are concentrated effectively suppresses spray combustion instability. The regions are identified as areas where interactions between distinct vortical structures are very strong. These regions serve as hubs that enhance intervortex interactions, facilitating the persistence of the organized structure. The sustained presence of such a structure strengthens the coupling between acoustic pressure and heat release rate fluctuations, forming a feedback mechanism that maintains combustion instability. This coupling is disrupted by placing an obstacle in the region of connector communities, leading to the suppression of spray combustion instability. Our results align with the findings of Sahay *et al.* [38], who demonstrated that vortical communities in a turbulent combustor exhibit strong intercommunity interactions during gaseous combustion instability. They identified critical flow regions through network analysis, showing that targeted interventions in these regions can mitigate combustion instability. Similarly, our study shows

that the disruption of connector communities effectively suppresses spray combustion instability. These findings highlight the critical role of the turbulence network structure in elucidating the driving mechanism and offer important insights into network-based strategies for suppressing combustion instability.

In this work, we have conducted a numerical study to clarify the network dynamics and construct a method to suppress spray combustion instability in a backward-facing step combustor from the perspective of a complex network. The findings obtained in this study can be summarized as follows: The scale-free topology in the turbulence network is intrinsically linked to the formation of a large-scale organized vortex. Hubs emerge and establish strong interactions within the network, maintaining the scale-free topology. This underscores the essential role of scale-free topology in the sustainment of combustion instability. In addition, the spatiotemporal evolution of node strength exhibits almost periodic fluctuations. This periodicity corresponds to the formation and collapse cycle of a large-scale organized vortex, suggesting that the turbulence network effectively captures the temporal characteristics of vortex dynamics. The availability of this framework to reveal such periodic behavior advances the physical understanding of vortex-driven combustion instabilities. Our study shows that the turbulence network not only characterizes the structural organization of turbulent flows but also provides deeper insights into the temporal evolution of dominant flow structures. Previous studies [25,35] on the control of combustion instability using the turbulence network have underscored that the primary hubs of the turbulence network significantly affect the spatiotemporal dynamics of the overall flow field during combustion instability. The disruption of the primary hubs by local injections of steady air jets into high-vorticity regions has been shown to be effective in suppressing gaseous combustion instability in swirl-stabilized and bluff body–stabilized combustors. Those studies [25,35] have provided a foundational framework for controlling combustion instability in the light of a complex network. In addition to the emphasis on the use of the turbulence network, the connector communities are useful for developing diverse and sophisticated methods to control combustion instability. A method for extracting the connector communities, as described in this paper, would be expected to be a promising strategy to control vortex-driven combustion instabilities in various combustors. Finally, there is an important issue concerning the suppression of spray combustion instability presented in this study. Placing the obstacle introduces modifications to the vorticity distribution in the flow field. We have observed a local increase in vorticity behind the obstacle due to flow separation and vortex shedding. At the present stage of our study, we infer that this disrupts the complete suppression of combustion instability. As shown in Fig. 7, the obstacle significantly reduces the strength of thermoacoustic power sources, suggesting the disruption of thermoacoustic coupling. In our next study, we plan to conduct numerical simulations in the cases of different geometries and sizes of the obstacle to gain a deeper understanding of the suppression mechanism of spray combustion instability.

IV. SUMMARY

We have numerically studied the network dynamics and suppression of spray combustion instability in a backward-facing step combustor, focusing on the behavior of a large-scale organized vortex driven by the growth of the shear layer at the edge of the backward-facing step. A scale-free topology appears, disappears, and reappears in the turbulence network constructed from the vorticity field. The collapse of a large-scale organized vortex leads to the loss of the scale-free topology and strongly affects the spatially irregular retention of primary hubs in the turbulence network. The probability density function of the lifetime of the scale-free topology exhibits a power-law decay. Spray combustion instability is significantly suppressed by placing an obstacle at the location where the connector communities are mostly formed in the turbulence network. This location is determined by estimating the participation coefficient for the communities. The suppression of spray combustion instability is clearly identified by the spatially averaged node strength in the acoustic-energy-flux-based spatial network and the recurrence rate in symbolic recurrence plots.

ACKNOWLEDGMENTS

We sincerely thank Dr. J. Nagao (Japan Aerospace Exploration Agency) and Mr. H. Hashiba (Tokyo University of Science) for implementing this study and stimulating discussions on the suppression of spray combustion instability. This work was partially supported by Japan Society for the Promotion of Science KAKENHI (Grants No. 22H00192 and No. 23K22691) and by the Ministry of Education, Culture, Sports, Science and Technology via the Program for Promoting Research on the Supercomputer Fugaku (Development of the Smart design system on the supercomputer Fugaku in the era of Society 5.0) (Grant No. JPMXP1020210316). This research used the computational resources of the supercomputer Fugaku provided by the RIKEN Center for Computational Science (Project No. hp240205).

DATA AVAILABILITY

The data that support the findings of this article are not publicly available. The data are available from the authors upon reasonable request.

[1] T. C. Lieuwen and V. Yang, *Combustion Instabilities in Gas Turbine Engines: Operational Experience, Fundamental Mechanisms, and Modeling* (American Institute of Aeronautics and Astronautics, 2005).

[2] J. O. Keller, L. Vaneveld, D. Korschelt, G. L. Hubbard, A. F. Ghoniem, J. W. Daily, and A. K. Oppenheim, Mechanism of instabilities in turbulent combustion leading to flashback, AIAA J. **20**, 254 (1982).

[3] D. A. Smith and E. E. Zukoski, 21st Joint Propulsion Conference, Monterey, CA, Technical Report AIAA-85-1248, 1985.

[4] T. J. Poinsot, A. C. Trouve, D. P. Veynante, S. M. Candel, and E. J. Esposito, Vortex-driven acoustically coupled combustion instabilities, J. Fluid Mech. **177**, 265 (1987).

[5] D. Thibaut and S. Candel, Numerical study of unsteady turbulent premixed combustion: Application to flashback simulation, Combust. Flame **113**, 53 (1998).

[6] K. C. Schadow and E. Gutmark, Combustion instability related to vortex shedding in dump combustors and their passive control, Prog. Energy Combust. Sci. **18**, 117 (1992).

[7] R. Sampath and S. R. Chakravarthy, Investigation of intermittent oscillations in a premixed dump combustor using time-resolved particle image velocimetry, Combust. Flame **172**, 309 (2016).

[8] N. B. George, V. R. Unni, M. Raghunathan, and R. I. Sujith, Pattern formation during transition from combustion noise to thermoacoustic instability via intermittency, J. Fluid Mech. **849**, 615 (2018).

[9] M. E. J. Newman, *Networks: An Introduction* (Oxford University Press, 2010).

[10] A.-L. Barabási, *Network Science* (Cambridge University Press, 2016).

[11] L. Lacasa, B. Luque, F. Ballesteros, J. Luque, and J. C. Nuño, From time series to complex networks: The visibility graph, Proc. Natl. Acad. Sci. USA **105**, 4972 (2008).

[12] J. Zhang and M. Small, Complex network from pseudoperiodic time series: Topology versus dynamics, Phys. Rev. Lett. **96**, 238701 (2006).

[13] N. Marwan, M. C. Romano, M. Thiel, and J. Kurths, Recurrence plots for the analysis of complex systems, Phys. Rep. **438**, 237 (2007).

[14] M. McCullough, M. Small, T. Stemler, and H. H.-C. Iu, Time lagged ordinal partition networks for capturing dynamics of continuous dynamical systems, Chaos **25**, 053101 (2015).

[15] K. Taira, A. G. Nair, and S. L. Brunton, Network structure of two-dimensional decaying isotropic turbulence, J. Fluid Mech. **795**, R2 (2016).

[16] G. Iacobello, L. Ridolfi, and S. Scarsoglio, A review on turbulent and vortical flow analyses via complex networks, Physica A **563**, 125476 (2021).

[17] K. Taira and A. G. Nair, Network-based analysis of fluid flows: Progress and outlook, Prog. Aerosp. Sci. **131**, 100823 (2022).

[18] R. I. Sujith and S. A. Pawar, *Thermoacoustic Instability* (Springer, 2021).

[19] M. Murugesan and R. I. Sujith, Combustion noise is scale-free: Transition from scale-free to order at the onset of thermoacoustic instability, J. Fluid Mech. **772**, 225 (2015).

[20] Y. Okuno, M. Small, and H. Gotoda, Dynamics of self-excited thermoacoustic instability in a combustion system: Pseudo-periodic and high-dimensional nature, Chaos **25**, 043107 (2015).

[21] V. Godavarthi, S. A. Pawar, V. R. Unni, R. I. Sujith, N. Marwan, and J. Kurths, Coupled interaction between unsteady flame dynamics and acoustic field in a turbulent combustor, Chaos **28**, 113111 (2018).

[22] S. Murayama, H. Kinugawa, I. T. Tokuda, and H. Gotoda, Characterization and detection of thermoacoustic combustion oscillations based on statistical complexity and complex-network theory, Phys. Rev. E **97**, 022223 (2018).

[23] S. Murayama and H. Gotoda, Attenuation behavior of thermoacoustic combustion instability analyzed by a complex-network-and synchronization-based approach, Phys. Rev. E **99**, 052222 (2019).

[24] Y. Guan, M. Murugesan, and L. K. B. Li, Strange nonchaotic and chaotic attractors in a self-excited thermoacoustic oscillator subjected to external periodic forcing, Chaos **28**, 093109 (2018).

[25] A. Krishnan, R. I. Sujith, N. Marwan, and J. Kurths, Suppression of thermoacoustic instability by targeting the hubs of the turbulent networks in a bluff body stabilized combustor, J. Fluid Mech. **916**, A20 (2021).

[26] K. Asami, T. Kawada, S. Kishiya, and H. Gotoda, Dynamic behavior and driving region of thermoacoustic combustion oscillations in a swirl-stabilized turbulent combustor, Europhys. Lett. **139**, 13001 (2022).

[27] Y. Guan, K. Moon, K. T. Kim, and L. K. B. Li, Synchronization and chimeras in a network of four ring-coupled thermoacoustic oscillators, J. Fluid Mech. **938**, A5 (2022).

[28] J. Zheng, Y. Guan, L. Xu, X. Xia, L. K. B. Li, and F. Qi, Scale-free topology of vortical networks in a turbulent thermoacoustic system, Phys. Rev. Fluids **9**, 033202 (2024).

[29] S. Tandon and R. I. Sujith, Multilayer network analysis to study complex inter-subsystem interactions in a turbulent thermoacoustic system, J. Fluid Mech. **966**, A9 (2023).

[30] T. Kitano, K. Kaneko, R. Kurose, and S. Komori, Large-eddy simulations of gas- and liquid-fueled combustion instabilities in back-step flows, Combust. Flame **170**, 63 (2016).

[31] A. L. Pillai, J. Nagao, R. Awane, and R. Kurose, Influences of liquid fuel atomization and flow rate fluctuations on spray combustion instabilities in a backward-facing step combustor, Combust. Flame **220**, 337 (2020).

[32] J. Nagao, A. L. Pillai, and R. Kurose, Investigation of temporal variation of combustion instability intensity in a back step combustor using LES, J. Therm. Sci. Technol. **15**, JTST0036 (2020).

[33] K. Kato, H. Hashiba, J. Nagao, H. Gotoda, Y. Nabae, and R. Kurose, Dynamic behavior and driving region of spray combustion instability in a backward-facing step combustor, Phys. Rev. E **110**, 024204 (2024).

[34] K. Kawano, H. Gotoda, Y. Nabae, Y. Ohmichi, and S. Matsuyama, Complex-network analysis of high-frequency combustion instability in a model single-element rocket engine combustor, J. Fluid Mech. **959**, A1 (2023).

[35] T. Kurosaka, S. Masuda, and H. Gotoda, Attenuation of thermoacoustic combustion oscillations in a swirl-stabilized turbulent combustor, Chaos **31**, 073121 (2021).
[36] Y. Mori, S. Kishiya, T. Kurosaka, and H. Gotoda, Feedback coupling and early detection of thermoacoustic combustion instability, Phys. Rev. Appl. **19**, 034097 (2023).
[37] R. Guimerà and L. A. N. Amaral, Functional cartography of complex metabolic networks, Nature **433**, 895 (2005).
[38] A. Sahay, M. G. Meena, and R. I. Sujith, Insights into the interplay between hydrodynamic and acoustic fields in a turbulent combustor via community-based dimensionality reduction of vortical networks, arXiv:2311.12541.
[39] T.-W. Lee, J. E. Park, and R. Kurose, Determination of the drop size during atomization of liquid jets in cross flows, At. Sprays **28**, 241 (2018).
[40] J. Bellan and K. Harstad, Analysis of the convective evaporation of nondilute clusters of drops, Int. J. Heat Mass Transf. **30**, 125 (1987).
[41] R. S. Miller, K. Harstad, and J. Bellan, Evaluation of equilibrium and non-equilibrium evaporation models for many-droplet gas-liquid flow simulations, Int. J. Multiphase Flow **24**, 1025 (1998).
[42] R. S. Miller and J. Bellan, Direct numerical simulation of a confined three-dimensional gas mixing layer with one evaporating hydrocarbon-droplet-laden stream, J. Fluid Mech. **384**, 293 (1999).
[43] M. G. Meena and K. Taira, Identifying vortical network connectors for turbulent flow modification, J. Fluid Mech. **915**, A10 (2021).
[44] V. D. Blondel, J. L. Guillaume, R. Lambiotte, and E. Lefebvre, Fast unfolding of communities in large networks, J. Stat. Mech. **10**, P10008 (2008).
[45] L. G. S. Jeub, M. Bazzi, I. S. Jutla, and P. J. Mucha, A generalized Louvain method for community detection implemented in MATLAB, 2011–2017, https://ljeub.github.io/code.html.
[46] Y. Mori, T. Kawada, S. Fukuda, and H. Gotoda, Nonlinear dynamics of attenuation behavior in combustion oscillations in a swirl-stabilized combustor, Proc. Combust. Inst. **39**, 4671 (2023).
[47] R. Ueta, H. Gotoda, H. Okamoto, K. Kawano, T. Shoji, and S. Yoshida, Interaction of acoustic pressure and heat release rate fluctuations in a model rocket engine combustor, Phys. Rev. E **110**, 014202 (2024).